

Electronic stopping power of slow-light channeling ions in ZnTe from first principlesChang-kai Li,^{1,2} Fei Mao,³ Feng Wang,⁴ Yan-long Fu,^{1,2} Xiao-ping Ouyang,⁶ and Feng-Shou Zhang^{1,2,5,*}¹*The Key Laboratory of Beam Technology and Material Modification of the Ministry of Education, College of Nuclear Science and Technology, Beijing Normal University, Beijing 100875, China*²*Beijing Radiation Center, Beijing 100875, China*³*School of Nuclear Science and Technology, University of South China, Hengyang 421001, China*⁴*School of Physics, Beijing Institute of Technology, Beijing 100081, China*⁵*Center of Theoretical Nuclear Physics, National Laboratory of Heavy Ion Accelerator of Lanzhou, Lanzhou 730000, China*⁶*Northwest Institute of Nuclear Technology, Xi'an 710024, China*

(Received 24 February 2017; published 22 May 2017)

Nonadiabatic dynamics simulations are performed to investigate the electronic stopping power of a helium ion moving through ZnTe crystalline thin films under channeling conditions. Using *ab initio* time-dependent density-functional theory, we found by direct simulation that electronic stopping power versus projectile velocity deviates from velocity proportionality and displays a transition between two velocity regimes for helium ions channeling along middle crystalline axes in $\langle 100 \rangle$ and $\langle 111 \rangle$ channels and also in a $\langle 110 \rangle$ channel with low-impact parameters. This transition causes a change in the slope of the energy loss versus ion velocity curve at a characteristic velocity related to the impact parameter and the lattice plane spacing. It may be an indication of extra energy loss channel beyond the electron-hole excitation. To analyze it, we checked the charge transfer between the moving projectiles and host atoms. It is found that the soft transition between two velocity regimes can be attributed to the resonant coherent excitation stimulated by the time-periodic potential experienced by the channeling ion and also the charge exchange in close encounters between Helium ion and host atoms.

DOI: [10.1103/PhysRevA.95.052706](https://doi.org/10.1103/PhysRevA.95.052706)**I. INTRODUCTION**

The interaction of ions with target atoms has been extensively studied ever since the discovery of the constituents of atoms in the beginning of the 20th century [1]. Stopping power (SP) is a quantitative measure of the interaction between the projectile and the target medium, defined as the energy transferred from the former to the latter per unit distance traveled through the material. Charged particles moving through solids gradually dissipate their energy due to the electronic excitation of the host atoms or the elastic collision with the target nuclei, which are known as electronic stopping power S_e and nuclear stopping power S_n , respectively. For particle velocities below the Fermi velocity of the target, nuclear and electronic stopping powers are both relevant, and the result of the interaction is a collision cascade [2]. The stopping maximum named the Bragg peak occurs shortly before the particle stops eventually. Thus, studying the energy transferred from slow ions (with velocities below the Bohr velocity) to the target material is of great importance to a wide range of research fields, from materials modification by irradiation in the nuclear and space industries to radiotherapy [3–14].

Fast-moving ions penetrate a great depth along channels between low-index crystallographic planes, slowing through collisions with electrons, until, finally, they hit a host atom, initiating a cascade of atomic displacements. This channeling phenomenon is widely applied to implantation technologies in semiconductor-device fabrication [15] and hardening tool steels by nitrogen implantation [16]. Channeling is key to the interpretation of high-energy ion scattering and recoil spectrometry [17]. It also plays a key role in irradiation damage

of crystalline materials in which incident high-energy particles in an encapsulation of nuclear waste may displace host atoms exceptionally long distances, significantly increasing the size of the damaged region [18].

Glancing collisions with host atoms confine the trajectory of a channeling ion, so most of its energy is lost through electronic excitation. Theoretical investigations of electronic stopping generally treat the host as a free-electron gas. Based on the homogeneous-electron-gas (HEG) model, S_e is predicted to be $S_e \propto v$ for $v < 1$ a.u. [19], which has been verified experimentally in many *sp*-bonded metals [20–23]. However, recent experimental studies on the deceleration of helium ions in thin Al films showed that the SP values for helium ions deviate from velocity proportionality. The results were understood by the charge-exchange process due to the repeated shifting of the $1s$ level of He up and down along the trajectory when getting close to Al atoms [24]. Nonlinearities of S_e are also found in noble metals such as Cu, Ag, and Au [25–27], but in these cases it is attributed to the threshold energy needed to excite the *d*-band electrons that are relatively tightly bound. In addition, materials with finite minimum excitation energy, such as noble gases, exhibit threshold effects experimentally [28]; the reason was interpreted to be the quantization of the target energy levels [29]. Furthermore, threshold effects were also discovered in insulators and semiconductors, such as LiF [30] and Ge [31]. It should be noted that Fermi *et al.* [19] pointed out that, in the case of insulators, the linear velocity dependence of S_e is valid only in the limit that the energy transferred from the projectile to the electrons of the host atoms is greater than the band gap. In this paper we find, through direct simulation, a transition between two energy-loss regimes. The aim of this work is to investigate the S_e behavior of a II–VI compound semiconductor in the low-velocity regime under channeling conditions and study

*Corresponding author: fszhang@bnu.edu.cn

the potential mechanisms resulting in the deviation from the velocity proportionality prediction.

In the present work, we focus particularly on S_e of helium ions in ZnTe under channeling conditions. For this purpose, we follow the explicit time evolution of the electronic states of the host crystal as an external particle propagating through the system by means of time-dependent density-functional theory (TDDFT). The energy transmitted to the electrons from moving ions is also monitored. In this study, the projectiles are initially directed along the negative z axis with a given velocity. Once the transient related to the sudden start has disappeared, S_e is extracted as the average rate of change of the ion kinetic energy with the distance traveled by the projectile. It should be noted that ionic motion of ZnTe is neglected by fixing ionic positions in the equilibrium because it is supposed to play a marginal role over the total simulation time that is limited to several femtoseconds.

In the velocity regime between 0.1 and 1 a.u. S_e is generally dominant, while for a lower velocity, S_n becomes sizable. Experimentally, it is tough to extract the electronic component in such low velocity. However, in simulations it is possible to directly access S_e . In the present work, S_e was investigated under channeling conditions, where the projectiles do not encounter the target nuclei directly. The nuclear contribution to the stopping power, therefore, is negligibly small and can even be completely suppressed when the host atom is frozen in the equilibrium position.

This article is outlined as follows. In Sec. II, we briefly introduce the theoretical framework and the computational details. Results are presented and discussed in Sec. III, where we concentrate on the analysis of S_e . In the end, conclusions are drawn in Sec. IV.

II. MODEL AND METHODS

In order to characterize the collision behaviors of helium ions with the nuclei and electrons of ZnTe [28], the Ehrenfest coupled electron-ion dynamics combined with time-dependent density-functional theory (ED-TDDFT) [6,9,32–35] is exploited. In this theoretical framework, electrons are quantum mechanically represented by wave functions, and nuclei are explicitly treated as classical particles in coordinate space. This method allows for an excited electronic state *ab initio* molecular dynamics simulation. The ED-TDDFT can, in general, be defined by the following coupled differential equations (atomic units with $m = |e| = \hbar = 1$ are used in this paper unless otherwise stated):

$$M_I \frac{d^2 \vec{R}_I(t)}{dt^2} = - \int \Psi^*(x,t) [\nabla_I \hat{H}_e(\vec{r}, \vec{R}(t))] \Psi(x,t) dx - \nabla_I \sum_{I \neq J} \frac{Z_I Z_J}{|\vec{R}_I(t) - \vec{R}_J(t)|}, \quad (1)$$

$$i \frac{\partial \Psi(x,t)}{\partial t} = \hat{H}_e(\vec{r}, \vec{R}(t)) \Psi(x,t), \quad (2)$$

where M_I and Z_I denote the mass and charge of the I th nuclei, respectively, and $\vec{R}_I(t)$ describes the corresponding ionic position vector. $\Psi(x,t)$ is the many-body electron wave function in the time domain, for which we define $x \equiv \{x_j\}_{j=1}^N$,

with $x_j \equiv (\vec{r}_j, \sigma_j)$, where the coordinates \vec{r}_j and the spin σ_j of the j th electron are implicitly taken into account. Here N is the number of electrons of the system.

The electronic Hamiltonian is expressed as $\hat{H}_e(\vec{r}, \vec{R}(t))$, which depends on the instantaneous distribution of the positions of all the nuclei, $\vec{R}(t) \equiv \{\vec{R}_1(t), \dots, \vec{R}_M(t)\}$ (M is the number of nuclei of the system), and of all the electrons \vec{r} ; thus, it basically consists of the kinetic energy of electrons, the Coulomb potential, and the electron-nuclei potential, which can be formulated as

$$\hat{H}_e(\vec{r}, \vec{R}(t)) = - \sum_j \frac{1}{2} \nabla_j^2 + \sum_{i < j} \frac{1}{|\vec{r}_i - \vec{r}_j|} - \sum_{iI} \frac{Z_I}{|\vec{R}_I - \vec{r}_i|. \quad (3)$$

To solve Eq. (1) for the motion of the nuclei, one has to obtain knowledge of $\Psi(x,t)$, which typically causes the problem to be intractable. For this reason, we write the force that acts on each nucleus in terms of the electronic density $\rho(\vec{r}, t)$, which is the basic variable of TDDFT-based Ehrenfest dynamics (see Ref. [36] for a detailed description). As a consequence, Eq. (1) can be rewritten as

$$M_I \frac{d^2 \vec{R}_I(t)}{dt^2} = - \int \rho(\vec{r}, t) [\nabla_I \hat{H}_e(\vec{r}, \vec{R}(t))] d\vec{r} - \nabla_I \sum_{I \neq J} \frac{Z_I Z_J}{|\vec{R}_I(t) - \vec{R}_J(t)|}, \quad (4)$$

where $\rho(\vec{r}, t)$ is obtained by the summation running over all occupied electronic orbitals, i.e.,

$$\rho(\vec{r}, t) = \sum_{i=1}^N |\varphi_i(\vec{r}, t)|^2, \quad (5)$$

with $\varphi_i(\vec{r}, t)$ being the Kohn-Sham (KS) orbital for the i th electron.

Similarly, to obtain $\rho(\vec{r}, t)$ explicitly, instead of solving Eq. (2), we make use of the corresponding time-dependent KS equations, which provides an approximation to $\rho(\vec{r}, t)$,

$$\left[-\frac{1}{2} \nabla^2 - \sum_I \frac{Z_I}{|\vec{R}_I(t) - \vec{r}|} + \int \frac{\rho(\vec{r}', t)}{|\vec{r} - \vec{r}'|} d\vec{r}' + V_{xc}(\vec{r}, t) \right] \varphi_i(\vec{r}, t) = i \frac{\partial \varphi_i(\vec{r}, t)}{\partial t}, \quad (6)$$

where $V_{xc}(\vec{r}, t)$ is the time-dependent exchange-correlation potential, for which we use the adiabatic local-density approximation with Perdew-Wang analytic parametrization [37]. The other three terms on the left-hand side of Eq. (6) are, in order, the electronic kinetic, the electron-nucleus potential, and the Hartree potential. Since we are mainly interested in the low-velocity regime that is well below the core-electron excitation threshold, only valence electrons of Te and Zn are considered throughout this work. The coupling of valence electrons to ionic cores is described by using norm-conserving Troullier-Martins pseudopotentials. The ground state of the system is calculated with the projectile being placed outside the crystal, the electronic orbitals of which are used as initial states for dynamical calculations. Once the convergence of the ground

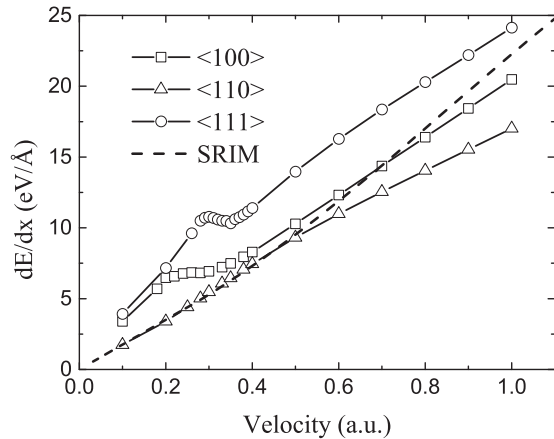


FIG. 1. Electronic stopping power for helium ions versus velocity along the center of three channels of ZnTe compared to the SRIM prediction (dashed line). The lines are guides to the eye.

state is achieved, the projectile is then released with the given initial velocity; meanwhile, the KS orbitals are propagated through the time-dependent KS equations by employing the approximated enforced time-reversal-symmetry method [38]. The ionic motion is obtained via the numerical solution of Eq. (4) by applying Verlet's algorithm.

The calculations were carried out using the OCTOPUS *ab initio* code package [39,40]. In the present work, the external potential, electronic density, and KS orbitals are discretized in a set of mesh grid points with a uniform spacing of 0.18 Å along the three spatial coordinates in the simulation box. To avoid artificial reflections of the electronic wave functions from the boundary, we use a complex-absorbing-potential boundary [41] during the collision process. For <110> and <111> channels a zinc-blende structured $2 \times 2 \times 2$ supercell comprising 32 Zn and 32 Te atoms is employed; for the <100> channel we exploit a $2 \times 2 \times 3$ supercell containing 48 Zn and 48 Te atoms. The lattice constant we used is 6.10 Å, which is identical to the measured value [42]. To ensure the stability of the computation, we use a time step of 0.001 fs. It should be noted that the numerical parameters have been carefully examined, and the chosen parameters are found to be a compromise between the convergence of results and the efficiency of the calculation.

III. RESULTS AND DISCUSSION

We computed S_e along the center of three different channels. Figure 1 presents our calculated results for S_e of helium ions in ZnTe with a velocity range of 0.1–1.0 a.u. For the sake of comparison, the prediction obtained from the SRIM-2013 database is also plotted in Fig. 1. It should be noted that SRIM results are obtained semiempirically by averaging over a number of different incident directions with distinct impact parameters; thus, it does not explicitly account for the channeling conditions studied in our calculations. For this reason, our calculated results are expected to follow a qualitative trend of SRIM data, which has been shown in several previous theoretical studies [13,43].

An interesting phenomenon we found in Fig. 1 is that, in the <110> channel, S_e has linear velocity scaling, which confirms the expected energy-dissipation mechanism caused by electron-hole pair excitation. While in the <100> and <111> channels a transition between two different velocity regimes can be observed, in both regimes S_e is velocity proportional; however, in the transition regime S_e is nearly velocity independent.

A. Effect of charge transfer on S_e

The deviation from the linear velocity dependence of S_e described above is similar to the experimental results of He^{2+} penetrating a homogeneous metal, Al in Ref. [24], where the nonlinear effect is interpreted to be the result of the charge-transfer process in close collisions. In the present work, we also find the nonlinearity of S_e is related to charge transfer, which is an additional energy-dissipation channel besides electron-hole pair excitation. Many mechanisms may contribute to the charge transfer. Besides the direct transitions such as excitation, ionization, and capture [44], the Auger process between the host atoms and ions also plays a pronounced role, in which an electron jumps from the valence band of the host atom to an ion bound state and vice versa. The energy released in such transitions is balanced by an electronic excitation in the medium or on the projectile [45]. Other possible mechanisms are resonant charge transfer and radiative decay processes of the projectiles. Since pseudopotentials are adopted in the present TDDFT simulation, Auger processes following the inner-shell vacancy cannot be considered. Nevertheless, because the kinetic ion energy in the present work is restricted to 25 keV/u and lower, according to the interpretation in Ref. [46], direct transition mechanisms are dominant in such a low-velocity regime; Auger processes following the inner-shell vacancy make a minor contribution to charge transfer.

In principle, both the neutralization and reionization processes can contribute to the decreasing of the projectile's kinetic energy, probably due to the promotion of electronic states of either the host atoms or the projectile itself.

As reported by Peñalba *et al.* [47], charge transfer is an important energy-loss channel, especially for projectiles around the stopping maximum. For protons with $v = 1$ a.u. in aluminum, charge transfer accounts for 15% of the total SP. However, it was not considered in the original SP theory that accounts for linear velocity dependence. The counterintuitive S_e versus the velocity of helium ions in Fig. 1 is studied by checking the charge-transfer behavior at different velocities.

As a first step, the time evolution of a helium ion moving through the <100> channel for a given velocity of 0.3 a.u. is visualized in 2 Four snapshots covering the entire collision process are presented. Before entering the crystal ($t = 0.341$ fs), the helium-ion projectile is a bare ion [Fig. 2(a)]. When the helium ion is getting close to the crystal ($t = 0.569$ fs) and penetrating along the channel ($t = 2.597$ fs), it exchanges charge with the host atoms [Figs. 2(b) and Line 166:433 Missing link [B4]: ... ion [Fig. 2(a)]. When...]. After traversing the ZnTe film ($t = 3.602$ fs), the exiting ion still retains some induced electrons [Fig. 2(d)]. The example in Fig. 2 could be qualitative evidence for the charge transfer during the collisions.

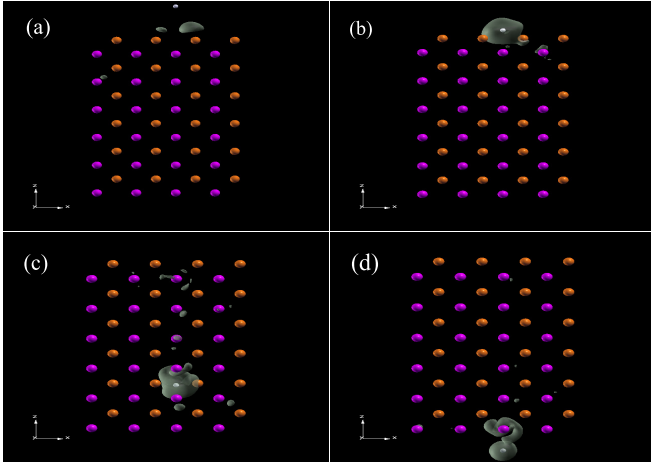


FIG. 2. Snapshots of time evolution of the electron density of a 0.3 a.u. He^{2+} ion moving through the ZnTe $\langle 100 \rangle$ channel (side view). (a) $t = 0.133$ fs; the ion is above the crystal. (b) $t = 0.569$ fs; the ion is entering the channel. (c) $t = 2.597$ fs; the ion is penetrating along the channel. (d) $t = 3.602$ fs; the leaving ion retains some electrons after the collision. The purple and orange circles represent Te and Zn layers, respectively, and the white circles are He ions; the gray region is the change in electron distribution caused by the intruding ion.

In order to quantitatively examine the electrons induced by the helium ion in real time, we integrated the valence charge density within the volume around the projectile ion with a radius of 1 Å [48] in the time-dependent calculation, from which the ground-state electron of the target in the corresponding volume has been subtracted, and we thus obtained the number of electrons induced by the helium ion, within the spherical volume around the helium ion in real time. A point to be noted is that the electron scattering process involving free electrons may also be included, where electrons pile up close to the projectile due to the attractive interaction between electrons and the He nuclei [49]. The choice of 1 Å as the integration radius is a compromise between various factors. In the present work, we are interested in finding the real-time electron occupying the intruding ion orbitals, and we get it through the discrepancy of the density, i.e., the change in the electron distribution around the ion between the time-dependent and ground-state calculations. In theory, a larger integration radius can be more effective to fully take a variety of mechanisms and also the highly occupied orbits into account. However, at the same time, it may include more free electrons and excited-state electrons of the host atoms that do not belong to the ion and also more excited-state electrons caused by the former steps, as shown in Fig. 2.

Electrons induced by the He^{2+} ion with different velocities moving along the middle axis of the $\langle 100 \rangle$ channel are presented in Fig. 3; the periodic variation in induced electrons reflects the periodicity of the crystal. As can be seen, in the low-velocity regime ($v \leq 0.3$ a.u.) the neutralization and reionization of the projectiles take place alternately along their trajectories. However, for velocities above 0.3 a.u. the electron exchange behavior is much less evident, especially in the latter part of trajectories in the channel. The oscillatory fraction, i.e., the strength of the charge-transfer behavior, is related to the stopping power caused by charge transfer. Based on the

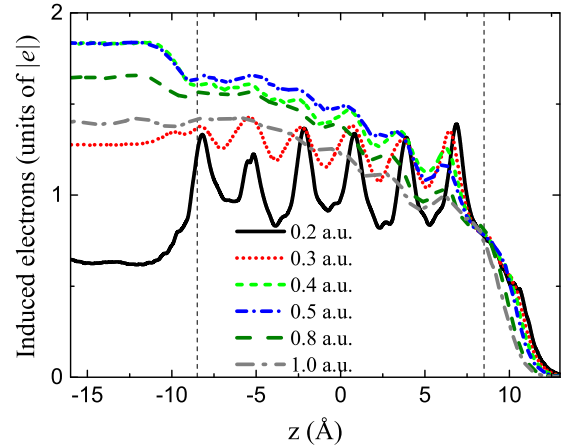


FIG. 3. Electron population change induced by the helium ion, within the spherical volume around the helium ion at different velocities versus z coordinates along the center of the $\langle 100 \rangle$ channel (see more details in the text). The region between the two vertical dashed lines is inside the ZnTe crystal.

homogeneous-gas model, if the electronic stopping power is caused only by electron-hole excitation, it should scale with velocity in the velocity regime below 1 a.u. In the present work charge transfer is viewed as an additional contribution to the stopping power, and it is more intense in the low-velocity regime ($v \leq 0.3$ a.u.). The relatively feeble charge-transfer behavior is expected to make a minor contribution to stopping power from charge transfer in the high-velocity regime ($v > 0.3$ a.u.). Considering charge transfer accounts for a noticeable share of S_e in the velocity regime below 1 a.u., the different charge-transfer behaviors in two velocity regimes are deemed to be one of the reasons accounting for the transition of stopping power between two velocity regimes, which is in agreement with the S_e results in Fig. 1.

Since the occupied He 1s level is strongly affected by the interaction distance [50–53], to investigate the effect of the impact parameter on charge exchange, we show in Fig. 4 the electron induced by He^{2+} ions moving along the middle axes of the $\langle 100 \rangle$, $\langle 110 \rangle$, and $\langle 111 \rangle$ channels at a given velocity of 0.3 a.u. As can be seen, the oscillation amplitude of induced electrons for helium ions in the $\langle 100 \rangle$ and $\langle 111 \rangle$ channels are relatively larger than that in the $\langle 110 \rangle$ channel; this could be due to the more compact atom distribution along the trajectories in these two channels. The distances between the ion trajectory and the nearest-neighbor atoms of the crystal are 1.53, 2.29, and 1.23 Å in the $\langle 100 \rangle$, $\langle 110 \rangle$, and $\langle 111 \rangle$ channels, respectively. A shorter distance between the projectile and host atoms means it is easier for the He 1s level to get promoted and shifted above the Fermi level E_F of ZnTe, which results in more effective neutralizing of He^{2+} ions and reionizing of He atoms. So the better linearity of S_e along the center of the $\langle 110 \rangle$ channel than in the other two channels in Fig. 1 can be attributed to less active charge-transfer behavior.

To further investigate the effect of the impact parameter on charge exchange, we have simulated two different trajectories in the $\langle 100 \rangle$ channel and three trajectories in the $\langle 110 \rangle$ channel, as shown in the insets in Fig. 5. The trajectories are chosen to sample different impact parameters (different closest distances

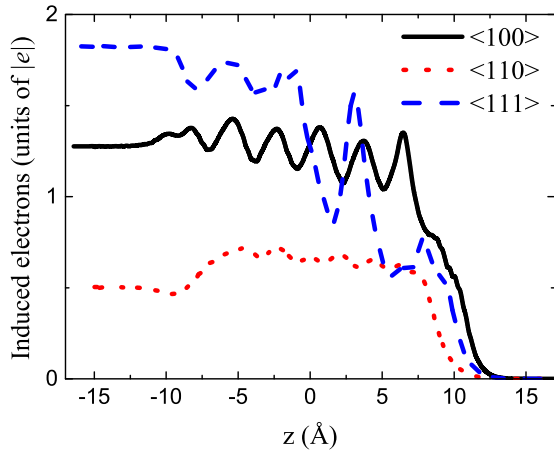


FIG. 4. Electron population change induced by the helium ion, within the spherical volume around the helium ion versus z coordinates for a given velocity of 0.3 a.u. along the center of the $\langle 100 \rangle$ (black solid line), $\langle 110 \rangle$ (red dotted line), and $\langle 111 \rangle$ (blue dashed line) channels. The range inside the crystal (from the top nuclei to the bottom nuclei) for the $\langle 100 \rangle$, $\langle 110 \rangle$, and $\langle 111 \rangle$ directions is $-8.4-8.4$, $-6.5-6.5$ and $-7.5-7.5$, respectively.

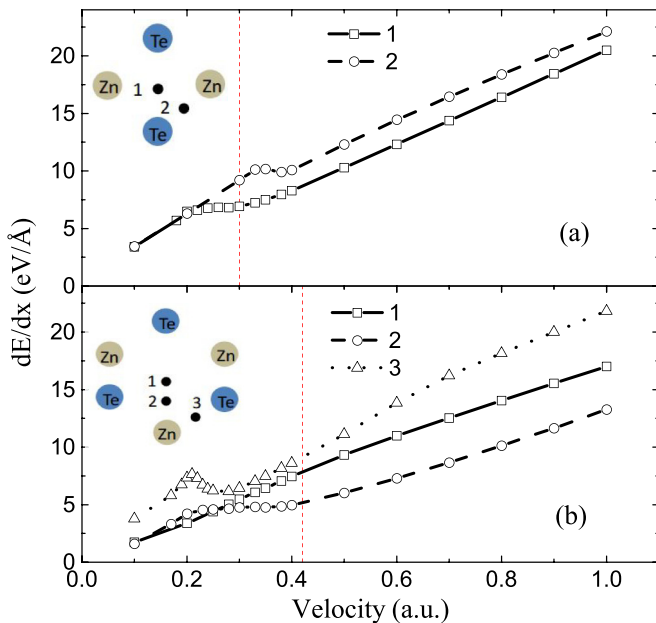


FIG. 5. Stopping power of helium ions in ZnTe as a function of the velocity (a) along two trajectories in the $\langle 100 \rangle$ channel and (b) three trajectories in the $\langle 110 \rangle$ channel. The lines are guides to the eye. The inset shows a sectional view of the $\langle 100 \rangle$ channel and the trajectories. The gray and blue circles represent host atoms in different transverse planes (defining the channel), while the black circles show the projectile positions for different impact parameters. The distances between the projectiles and the nearest-neighbor atoms of the crystal in the $\langle 100 \rangle$ channel are 1.53 and 1.08 Å, respectively. The distances between the projectiles and the nearest-neighbor atoms of the crystal in the $\langle 110 \rangle$ channel are 2.29, 1.53, and 1.32 Å respectively. The vertical red dashed line shows the threshold velocities for resonant coherent excitation of $\text{He}^0 1s \rightarrow 2p$ (see more details in the text).

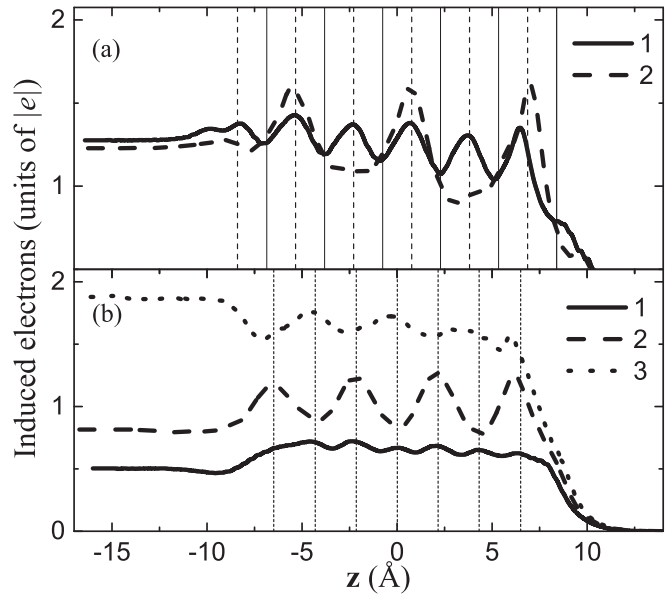


FIG. 6. Electron population change induced by the helium ion, within the spherical volume around the helium ion along trajectories with different impact parameters (a) in the $\langle 100 \rangle$ channel and (b) in the $\langle 110 \rangle$ channel for a given velocity of 0.3 a.u. The curves correspond to trajectories in Fig. 5. The vertical solid and dashed lines in (a) are the positions of Te and Zn layers, respectively. The vertical short-dashed lines in (b) are positions of crystalline layers comprising both Te and Zn atoms.

to any of the host atoms) within the channel. So trajectories in the center of the channel have the highest impact parameter, and trajectories close to the edge of the channel have the lowest impact parameter. For each trajectory we show the S_e behavior and the electron induced by the projectiles versus z coordinates for a given velocity of 0.3 a.u. For comparison, data along the center of the channels are also shown. Figure 5 shows the S_e behavior along different trajectories in the $\langle 100 \rangle$ and $\langle 110 \rangle$ channels. Figure 6 shows the corresponding charge-transfer profiles. As can be seen, a larger variation in the induced-electron population is observed for the trajectories with the low impact parameters than in the center of the channels. Moreover, the resulting nonlinearity of S_e versus velocity in Fig. 5 is more evident for the off-center channeling, especially in the $\langle 110 \rangle$ channel; the initially missing transition between two velocity regimes occurs in the off-center channeling cases.

B. Effect of resonant coherent excitation on S_e

Another important physical process for channeling ions is the resonant transition induced by the crystal pseudopotential [54,55]. The scenario describes that when swift atoms or ions traverse a crystal foil under channeling conditions, the periodic Coulomb field in the solid may result in electronic transitions of the projectile. Okorokov [56] predicted that such a periodic perturbation for a projectile atom, traveling with constant velocity v , gives rise to resonant excitation phenomena with enhanced transition probabilities, i.e., resonant coherent excitation (RCE) [57]. The influence of periodic perturbation on the electronic transitions can be evaluated quantitatively by the energy $\hbar\omega$, where the resulting frequency is associated

with the distance (denoted by d) between tetrahedral points in the channel and the impact velocity, i.e., $\omega = 2\pi|v|/d$. Taking into account the quantization of the electronic energy levels, a characteristic threshold velocity is expected to cause the electronic excitation on the projectile when traversing the crystal channel. The calculated threshold velocities for resonant coherent excitation of $\text{He}^0 1s \rightarrow 2p$ in the $\langle 100 \rangle$ and $\langle 110 \rangle$ channels is marked as vertical red dashed lines in Fig. 5.

In the present work, we found the threshold velocity depends strongly on the impact parameter and lattice plane spacing. As observed in Fig. 5, trajectories in the same channel (with identical lattice spacing but different impact parameters) have different threshold velocities. This result is in agreement with the interpretation in [57]: The energy levels of channeling ions are not quite the same as in the vacuum, being perturbed by the electric potential of the crystal. The electrostatic potential increases with displacement from the center of a channel, so the potential energy of an electron decreases. This potential lowers the electronic levels of the channeling ion. Since the higher-energy orbitals extend farther, they are affected more than the ground state, and the result is a decrease in the energy difference between levels. Therefore, one expects the threshold velocity to be smaller than the vacuum values. For $\langle 100 \rangle$ and $\langle 110 \rangle$ channels, the value of $\hbar\omega$ for the projectile with a speed of 1 a.u. is calculated to be 33.9 eV, which is beyond the ionization energy of a helium atom. A point that must be noted is that since the resonant excitations caused by RCE are between states on the same ion, its charge state changes only if ionization occurs. This point can be verified by the reduced number of electrons induced by the projectile with a velocity above 0.5 a.u. presented in Fig. 3.

As to the effect of RCE on S_e , according to the interpretation in [58], based on the tight-binding model, exciting electrons out of their ground state reduces the bond order, thus modifying both the energy of the system and the forces experienced by atoms. It is a reduction because the number of electrons in bonding states is reduced, while the number of electrons in antibonding states is increased through the excitation. Consequently, the stopping power is always expected to fall below the linear relationship at the onset of the RCE, which is in agreement with the results in the present work. It should be noted that according to the interpretation in Ref. [57], RCE is always accompanied by sharp peaks in energy-dependent measurements of ion charge states under channeling conditions. However, such sharp peaks are not observed in the present work, which may be due to finite-size effects [10]. In the present work, the channeling ion only experiences several rows of host atoms within 10 fs and below; one should allow time for a steady-state charge distribution caused by RCE to be established in the frame of the moving ion.

C. Direction dependence of S_e

Another finding in Fig. 1 is that S_e is remarkably orientation dependent, resulting in different channels having different magnitudes. To understand the dependence of S_e on the incident direction, Fig. 7 presents the ground-state electronic density and the axial force along the ion trajectory for helium ions at a velocity of 0.3 a.u. As shown in Eq. (2), the forces

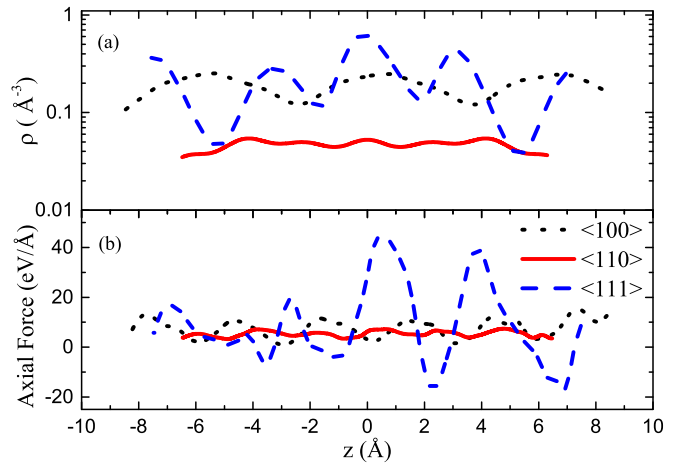


FIG. 7. (a) Electron densities and (b) axial force exerted on a helium ion for a given velocity of 0.3 a.u. versus z coordinates in ZnTe along the center of the $\langle 100 \rangle$ (black dotted lines), $\langle 110 \rangle$ (red solid lines), and $\langle 111 \rangle$ (blue dashed lines) channels.

on the nuclei (including the intruding ion) in TDDFT are evaluated using the time-dependent electron density $\rho(r,t)$ and the Coulomb interactions. It is noted, however, that a fraction of the computed oscillatory axial force is due to the interaction of the projectile with the undisturbed target potential, without any electronic excitation process. The periodic variation in the force reflects the periodicity of the crystal. The density values are obtained by averaging the electron density of the cylindrical ion track with a radius of 0.36 Å. It shows that the electronic concentration in the $\langle 110 \rangle$ channel is rarer than that of the other two channels. Electron density in the $\langle 100 \rangle$ and $\langle 111 \rangle$ channels does not differ significantly if averaged over the z axis, yielding 0.19 and 0.22 electron/Å³, respectively. This is consistent with S_e displayed in Fig. 1, suggesting that S_e in channeling conditions could be related to the average density along the projectile's trajectory, which corroborates and supports assumptions and approximations in the literature [59–62]. The trend of the axial force is similar to that of electron density, and there is a proportional relation between the two to some extent, which is in accordance with the density-functional-theory results [63] for the HEG model. The discrepancy in force between $\langle 110 \rangle$ and the other two channels is less evident than that of density, which may indicate that the uniformly distributed electron density is more effective in stopping the channeling ions.

IV. CONCLUSIONS

A first-principles theoretical study of the electronic stopping power of slow-light projectiles in ZnTe has been presented. The transition of the S_e slope between two velocity regimes was found, which was interpreted to be a consequence of charge transfer and RCE. The threshold of the transition has been verified to be related to impact parameter and crystalline structure. In fact, we have found this type of nonlinear behavior of stopping power versus velocity in many other materials with similar crystalline structure, such as CdTe, ZnSe, and CdSe, under channeling conditions; the results will be reported in future works. Another finding is that S_e is orientation dependent.

dent, and the electron density determines the magnitude of S_e , which is consistent with the assumptions of the HEG model.

Currently, TDDFT studies of the stopping power are restricted to systems of hundreds of atoms with pseudopotentials defined by “ions” (nucleus + core electrons) [7,13]. In the present work, only the uppermost valence electrons of Te and Zn were considered. However, the interpretation in Ref. [44] suggests that electron capture from the inner shell of tellurium might be a significant contribution to electron capture in the He^{2+} projectile. So the calculation is expected to be improved by consideration of the inner-shell electron. However, the computational resources needed for an all-electron TDDFT calculation like this work are currently unachievable. Still, it is an interesting subject for future work to explore.

Our results give further insight into describing the interaction between the ions and the target electrons without restrict-

ing the electrons to the adiabatic surface. To obtain a deeper understanding of the effect of charge transfer on inelastic energy loss, a thorough theoretical analysis of the dissipation mechanisms in combination with suitable experimental studies is highly desirable.

ACKNOWLEDGMENTS

Fruitful discussions with Dr. C. Z. Gao and Dr. W. Cheng are acknowledged. This work was supported by the National Natural Science Foundation of China under Grants No. 11635003, No. 11025524, and No. 11161130520, the National Basic Research Program of China under Grant No. 2010CB832903, and the European Commissions 7th Framework Programme (FP7-PEOPLE-2010-IRSES) under Grant Agreement Project No. 269131.

-
- [1] E. Rutherford, *Philos. Mag.* **21**, 669 (1911).
- [2] R. S. Averback and T. D. D. L. Rubia, *Solid State Phys.* **51**, 281 (1997).
- [3] J. E. Valdés, J. C. Eckardt, G. H. Lantschner, and N. R. Arista, *Phys. Rev. A* **49**, 1083 (1994).
- [4] E. A. Figueroa, E. D. Cantero, J. C. Eckardt, G. H. Lantschner, J. E. Valdés, and N. R. Arista, *Phys. Rev. A* **75**, 010901 (2007).
- [5] E. D. Cantero, G. H. Lantschner, J. C. Eckardt, and N. R. Arista, *Phys. Rev. A* **80**, 032904 (2009).
- [6] M. A. Zeb, J. Kohanoff, D. Sánchez-Portal, A. Arnau, J. I. Juaristi, and E. Artacho, *Phys. Rev. Lett.* **108**, 225504 (2012).
- [7] J. M. Pruneda, D. Sánchez-Portal, A. Arnau, J. I. Juaristi, and E. Artacho, *Phys. Rev. Lett.* **99**, 235501 (2007).
- [8] E. Artacho, *J. Phys. Condens. Matter* **19**, 275211 (2007).
- [9] A. P. Horsfield, D. R. Bowler, A. J. Fisher, T. N. Todorov, and M. J. Montgomery, *J. Phys. Condens. Matter* **16**, 3609 (2004).
- [10] D. R. Mason, J. L. Page, C. P. Race, W. M. C. Foulkes, M. W. Finnis, and A. P. Sutton, *J. Phys. Condens. Matter* **19**, 436209 (2007).
- [11] C. P. Race, D. R. Mason, and A. P. Sutton, *J. Phys. Condens. Matter* **21**, 115702 (2009).
- [12] A. M. Rutherford and D. M. Duffy, *J. Phys. Condens. Matter* **19**, 496201 (2007).
- [13] A. A. Correa, J. Kohanoff, E. Artacho, D. Sánchez-Portal, and A. Caro, *Phys. Rev. Lett.* **108**, 213201 (2012).
- [14] A. V. Krasheninnikov, Y. Miyamoto, and D. Tománek, *Phys. Rev. Lett.* **99**, 016104 (2007).
- [15] E. Rimini, *Ion Implantation: Basics to Device Fabrication* (Springer, New York, 1995).
- [16] J. R. Conrad, J. L. Radtke, R. A. Dodd, F. J. Worzala, and N. C. Tran, *J. Appl. Phys.* **62**, 4591 (1987).
- [17] L. J. V. Ijzendoorn, *Anal. Chim. Acta* **297**, 55 (1994).
- [18] I. Farnan, H. Cho, and W. J. Weber, *Nature (London)* **445**, 190 (2007).
- [19] E. Fermi and E. Teller, *Phys. Rev.* **72**, 399 (1947).
- [20] C. P. Race, D. R. Mason, M. W. Finnis, W. M. C. Foulkes, A. P. Horsfield, and A. P. Sutton, *Rep. Prog. Phys.* **73**, 116501 (2010).
- [21] J. E. Valdés, G. A. Tamayo, G. H. Lantschner, J. C. Eckardt, and N. R. Arista, *Nucl. Instrum. Methods Phys. Res., Sect. B* **73**, 313 (1993).
- [22] G. Martínez-Tamayo, J. C. Eckardt, G. H. Lantschner, and N. R. Arista, *Phys. Rev. A* **54**, 3131 (1996).
- [23] J. M. Pitarke and I. Campillo, *Nucl. Instrum. Methods Phys. Res., Sect. B* **164**, 147 (2000).
- [24] D. Primetzhofer, S. Rund, D. Roth, D. Goebel, and P. Bauer, *Phys. Rev. Lett.* **107**, 163201 (2011).
- [25] E. A. Figueroa, E. D. Cantero, J. C. Eckardt, G. H. Lantschner, M. L. Martiarena, and N. R. Arista, *Phys. Rev. A* **78**, 032901 (2008).
- [26] S. N. Markin, D. Primetzhofer, S. Prusa, M. Brunmayr, G. Kowarik, F. Aumayr, and P. Bauer, *Phys. Rev. B* **78**, 195122 (2008).
- [27] D. Primetzhofer, M. Spitz, S. N. Markin, E. Taglauer, and P. Bauer, *Phys. Rev. B* **80**, 125425 (2009).
- [28] R. Golser and D. Semrad, *Phys. Rev. Lett.* **66**, 1831 (1991).
- [29] P. L. Grande and G. Schiwietz, *Phys. Rev. A* **47**, 1119 (1993).
- [30] S. N. Markin, D. Primetzhofer, and P. Bauer, *Phys. Rev. Lett.* **103**, 113201 (2009).
- [31] D. Roth, D. Goebel, D. Primetzhofer, and P. Bauer, *Nucl. Instrum. Methods Phys. Res., Sect. B* **317**, 61 (2013).
- [32] E. K. U. Gross, J. F. Dobson, and M. Petersilka, in *Density Functional Theory II: Relativistic and Time Dependent Extensions*, edited by R. F. Nalewajski (Springer, Berlin, 1996), p. 81.
- [33] F. Calvayrac, P. G. Reinhard, E. Suraud, and C. A. Ullrich, *Phys. Rep.* **337**, 493 (2000).
- [34] J. L. Alonso, X. Andrade, P. Echenique, F. Falceto, D. Prada-Gracia, and A. Rubio, *Phys. Rev. Lett.* **101**, 096403 (2008).
- [35] J. L. Page, D. R. Mason, and W. M. C. Foulkes, *J. Phys. Condens. Matter* **20**, 125212 (2008).
- [36] A. Castro, M. Isla, J. I. Martínez, and J. A. Alonso, *Chem. Phys.* **399**, 130 (2012).
- [37] J. P. Perdew and Y. Wang, *Phys. Rev. B* **45**, 13244 (1992).
- [38] A. Castro and M. A. L. Marques, *Propagators for the Time-Dependent Kohn-Sham Equations* (Springer, Berlin, 2004), p. 197.
- [39] M. A. L. Marques, A. Castro, G. F. Bertsch, and A. Rubio, *Comput. Phys. Commun.* **151**, 60 (2003).
- [40] A. Castro, H. Appel, M. Oliveira, C. A. Rozzi, X. Andrade, F. Lorenzen, M. A. L. Marques, E. K. U. Gross, and A. Rubio, *Phys. Status Solidi B* **243**, 2465 (2006).

- [41] F. Wang, X. C. Xu, X. H. Hong, J. Wang, and B. C. Gou, *Phys. Lett. A* **375**, 3290 (2011).
- [42] Y. Lalignant, G. Ferey, G. Heger, and J. Pannetier, *Z. Anorg. Allg. Chem.* **553**, 163 (1987).
- [43] A. Schleife, Y. Kanai, and A. A. Correa, *Phys. Rev. B* **91**, 014306 (2015).
- [44] G. Schiwietz and P. L. Grande, *Phys. Rev. A* **84**, 052703 (2011).
- [45] R. D. Muiño, *Nucl. Instrum. Methods Phys. Res., Sect. B* **203**, 8 (2003).
- [46] C. L. Zhang, X. H. Hong, F. Wang, Y. Wu, and J. G. Wang, *Phys. Rev. A* **87**, 032711 (2013).
- [47] M. Peñalba, A. Arnau, P. M. Echenique, F. Flores, and R. H. Ritchie, *Europhys. Lett.* **19**, 45 (1992).
- [48] C. Z. Gao, J. Wang, and F. S. Zhang, *Chem. Phys.* **410**, 9 (2013).
- [49] P. Echenique, R. Nieminen, and R. Ritchie, *Solid State Commun.* **37**, 779 (1981).
- [50] N. P. Wang, E. A. García, R. Monreal, F. Flores, E. C. Goldberg, H. H. Brongersma, and P. Bauer, *Phys. Rev. A* **64**, 012901 (2001).
- [51] S. Wethekam, D. Valdés, R. C. Monreal, and H. Winter, *Phys. Rev. B* **78**, 075423 (2008).
- [52] R. Monreal, E. Goldberg, F. Flores, A. Narmann, H. Derks, and W. Heiland, *Surf. Sci. Lett.* **211**, 271 (1989).
- [53] D. Primetzhofer, D. Goebel, and P. Bauer, *Nucl. Instrum. Methods Phys. Res., Sect. B* **317**, 8 (2013).
- [54] P. M. Echenique, F. Flores, and R. H. Ritchie, *Nucl. Instrum. Methods Phys. Res., Sect. B* **33**, 91 (1988).
- [55] F. Sols and F. Flores, *Phys. Rev. B* **30**, 4878 (1984).
- [56] V. V. Okorokov, *Yadern Fiz* **2**, 349 (1965).
- [57] C. D. Moak, S. Datz, O. H. Crawford, H. F. Krause, P. F. Dittner, J. G. d. Campo, J. A. Biggerstaff, P. D. Miller, P. Hvelplund, and H. Knudsen, *Phys. Rev. A* **19**, 977 (1979).
- [58] D. R. Mason, C. P. Race, M. H. F. Foo, A. P. Horsfield, W. M. C. Foulkes, and A. P. Sutton, *New J. Phys.* **14**, 073009 (2012).
- [59] N. P. Wang and I. Nagy, *Phys. Rev. A* **56**, 4795 (1997).
- [60] N. P. Wang, I. Nagy, and P. M. Echenique, *Phys. Rev. B* **58**, 2357 (1998).
- [61] H. Winter, J. I. Juaristi, I. Nagy, A. Arnau, and P. M. Echenique, *Phys. Rev. B* **67**, 245401 (2003).
- [62] L. Martingondre, G. A. Bocan, M. Blancorey, M. Alducin, J. I. Juaristi, and R. D. Muiño, *J. Phys. Chem. C* **117**, 9779 (2013).
- [63] P. M. Echenique, R. M. Nieminen, J. C. Ashley, and R. H. Ritchie, *Phys. Rev. A* **33**, 897 (1986).